Heat Hunting in a Freezer: Direct Measurement of Quasiparticle Diffusion in Superconducting Nanowire

M. Zgirski,[1,*] M. Foltyn,[1] A. Savin,[2,3] A. Naumov,[1] and K. Norowski[1]

[1] *Institute of Physics, Polish Academy of Sciences, Aleja Lotnikow 32/46, Warsaw PL 02668, Poland*

[2] *Low Temperature Laboratory, Department of Applied Physics, Aalto University School of Science, Aalto FI-00076, Finland*

[3] *QTF Centre of Excellence, Department of Applied Physics, Aalto University School of Science, Aalto FI-00076, Finland*

(Received 25 October 2019; revised 14 September 2020; accepted 18 September 2020; published 15 October 2020)

Propagation and relaxation of nonequilibrium quasiparticles in superconductors are fundamental for functioning of numerous nanoscale devices, enabling operation of some of them, and limiting the performance of others. The quasiparticles heated above lattice temperature may relax locally via phonon or photon-emission channels, or diffuse over appreciable distances in a nanostructure altering the functionality of their remote components. Tracing quasiparticles experimentally in real-time domain has remained a challenging task owing to their rapid dynamics. With electronic nanothermometry, based on probing of the temperature-dependent switching current of a superconducting nanobridge, we monitor heat pulse carried by a flux of nonequilibrium quasiparticles as it passes by our detector with a noise-equivalent temperature of 10 mK/$\sqrt{N}$, where N is the number of pulses probing the bridge (typically $N = 10\,000$), and temporal resolution of a single nanosecond. The measurement provides the picture of quasiparticle diffusion in a superconducting aluminum strip and direct determination of the diffusion constant D equal to 100 cm^2/s with no energy dependence visible.

DOI: 10.1103/PhysRevApplied.14.044024

I. INTRODUCTION

The superconducting state at a finite temperature is characterized by equilibrium population of not paired electrons, known for their finite lifetime and tendency to recombine back into Cooper pairs as quasiparticles (QPs). When a metallic nanostructure is cooled down towards absolute zero, energy transfer between electrons and phonons becomes much less efficient resulting in thermal decoupling of the two systems [1]. If electrons absorb energy due to the Joule heating or irradiation with photons, they acquire temperature higher than that of the lattice. Such overheated electrons, often referred to as hot electrons, in a superconductor are known as nonequilibrium QPs. They diffuse in a nanostructure until they emit phonons [2] or photons [3] and adopt equilibrium occupation of states corresponding to the lattice temperature. The diffusion process, albeit much slower than ballistic propagation of electrons with the Fermi velocity v_F, has been too fast for existing experimental techniques to be traced in real-time domain. Dynamical thermal properties of nanostructures at low temperatures were mostly investigated by assumption of heat-flow models describing thermal steady states, involving thermometry based on normal-metal–insulator–superconducting tunnel junctions [4–6], measurement of superconducting quantum interference device (SQUID) noise [7] and Coulomb blockade in quantum dots [8]. Since thermal and electrical attributes are intimately related, it was possible to get access to some thermal parameters by performing electrical transport measurements, e.g., the Einstein formula for a degenerate conductor relates a diffusion constant and electrical conductivity [4], the Wiedemann-Franz law relates electrical and thermal conductivities [9,10]. There were also successful measurements of the thermal transients with temperature sensors embedded in rf or microwave resonators [11,12] with a noise-equivalent temperature (NET) ranging from 90 μK/$\sqrt{\text{Hz}}$ [13] to 10 μK/$\sqrt{\text{Hz}}$ [12], respectively. They demonstrated real-time traces of the electron temperature for QPs releasing their excess energy to phonons. Owing to a typical bandwidth of 10 MHz, experimentalists were able to trace thermal relaxation times down to approximately 300 ns at temperatures below 0.5 K [14, 15]. Utilizing recently developed switching thermometry with Josephson junction [16], we present direct measurement of the QP diffusion in the superconducting nanostructure achieving resolution below 100 μK. Our study

*zgirski@ifpan.edu.pl

shows that tracing thermal processes in nanoscale with nanosecond resolution is possible and opens alternative perspectives for investigation of thermodynamics of low-temperature quantum circuits. A proper understanding of thermal transients is essential for failure-free functioning of cryogenic nanodevices, involving design and development of nanoscale calorimeters and bolometers [17–19], microcoolers [20], and qubits. Devices like single-electron boxes, proposed as building blocks of modern current standard, suffer from the presence of QPs responsible for leakage currents and resulting "counting errors," that spoil metrological applications. Similarly, microcoolers' performance is degraded due to the QP poisoning. The QPs are also known to have a detrimental influence on the coherence times of superconducting [21] or Majorana [22,23] qubits. On the other hand, the creation of QPs due to photon absorption makes it possible for superconducting bolometers to detect incident radiation with the lifetime of QPs imposing an intrinsic limitation on the bandwidth of such sensors [14]. Our study may offer alternative ways for advancement of the emergent fields of quantum thermodynamics [24] and phase-coherent caloritronics [25]. The latter involves generation and manipulation of heat currents to demonstrate innovative-concept devices [26,27]. Harnessing heat-current pulses as thermal counterparts of electrical signals could extend the discipline beyond steady-state investigations and provide a competitive alternative for phononics [28] and spin caloritronics [29].

II. SAMPLE

We fabricate a device with a normal-metal heater galvanically connected to a superconducting aluminum nanowire interrupted with a nanobridge (Fig. 1, [30]). The bridge is a sensitive thermometer and the Joule-heated copper island, placed $X_T = 60$ μm away, is a source of nonequilibrium QPs, where electrons are promoted to higher energy levels with the local Fermi-Dirac distribution characterized by temperature elevated above the phonon temperature. The distribution relaxes towards equilibrium with phonons only gradually and relaxation process may require seconds in a few milikelvin temperature [31–33]. Hot electrons move with v_F (equal to a few percent of speed of light) but due to scattering on different lattice defects, i.e., grain boundaries, sample surface, or impurities, their spreading in nanostructure is not so fast but instead takes on diffusive character. Qualitatively, in its random walk an average hot electron bounces off each approximately 2–100 nm (a length known as an elastic mean free path l_{MFP}) and after many collisions covers distance given by Einstein-Smoluchowski law: $\langle l^2 \rangle = D\tau$, where $\langle l^2 \rangle$ is a mean square displacement from a starting point after time τ and D is the diffusion constant. It accounts for approximately 1–1000 ns required for hot electrons to spread in a conventional microstructure with size 10–100 μm. For the presented sample, hot electrons diffuse along the wire transporting the heat away from the copper island. On the way they lose energy to phonons ($\dot{q}_{\mathrm{EP}}$

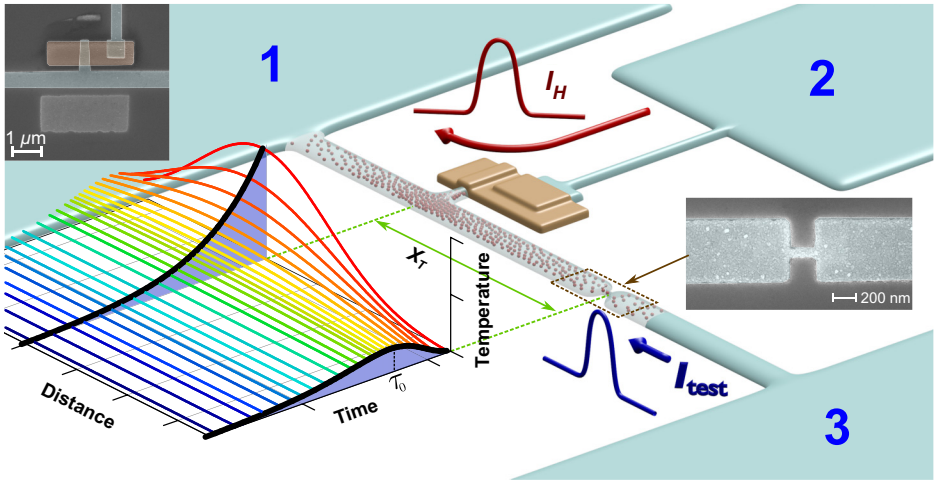

FIG. 1. Pictorial layout of the experiment. Hot electrons are created in the heater by applying short current pulse I_H (approximately 10 ns long) flowing between ports 1 and 2. QPs start diffusing along the nanowire. Qualitatively, their population at the bridge location is derived from the time-evolving Gaussian profile as $N_T(\tau) \sim (1/\sqrt{2\pi D\tau})\exp(-X_T^2/2D\tau)$ within the free-particle diffusion model, with the maximum of hot-electron signal indicated at $\tau_0 = X_T^2/D$. Similarly, hot-electron population in the heater is $N_H(\tau) \sim 1/\sqrt{2\pi D\tau}$. Taking into account annihilation of nonequilibrium QP due to interaction with phonons and "colder" QPs allows us to describe the temperature variations in the bridge quantitatively (see description in the text), but introduces only minor changes to temporal dynamics with almost the same time marking the onset and the maximum of the QP signal at the bridge. The insets show the SEM images of the copper heater and the aluminum nanobridge of the measured nanostucture. The testing pulse I_{test}, flowing between ports 1 and 3 is used to test the bridge temperature (see description in the text).

is the energy flux to phonons) and equilibrate with local QPs occupying lower-energy states characterized by lower temperature. We assume that in each section of the wire electrons are described with equilibrium Fermi-Dirac distribution and their temperature is well defined. The energy required for the hot-electron flux to equilibrate with local electrons is accounted for by the heat capacity C_p of the QPs in the superconducting state. Finally, QPs arrive to the nanobridge, whose switching current is sensitive to their local population.

III. SWITCHING THERMOMETRY

We use and further develop nanosecond thermometry based on stochastic switching of a Josephson junction from superconducting to normal state [16,34]. A particular type of Josephson junction, a superconducting aluminum nanobridge known in the literature as the Dayem bridge, is well tailored for tracing rapid changes in temperature, which are expected when hot electrons propagate across the nanostructure. The bridge is probed with train of N current pulses (see I_{test} pulse sent between port 1 and 3 in Fig. 1) in the experimental setup presented within the Supplemental Material [30]. In response to each pulse it may either remain in the superconducting state or transit to the normal state. The switching process is both current and temperature dependent. Number of switching events n increases with amplitude of the probing pulse and switching probability $P = n/N$ renders a familiar S-shaped curve. Such an S curve is centered at lower current amplitudes for higher temperatures [Fig. 2(a)]. The variation of S-curve position with temperature [Fig. 2(b)] and its slope define the temperature responsivity $\Delta P/\Delta T_e$ at constant testing current amplitude [Figs. 2(e) and 2(f)]. Alternatively, temperature can be derived by associating unique current amplitude corresponding to $P = 0.5$ switching probability with temperature [Fig. 2(b)]. We call these two switching-thermometry methods "Temperature from probability" and "Temperature from switching current," respectively.

A. Temperature from probability

During a thermal transient, when a nanobridge is probed with pulses of a constant amplitude, excess values of the switching probability ΔP correspond to departures of electron temperature ΔT_e from lattice temperature T_{ph}. In the linear range of an S curve ($\delta P/\delta I_{\text{test}} = \text{const}$), covering the interval $0.2 < P < 0.8$, ΔP is proportional to ΔT_e. We tune switching current to obtain $P = 0.2$ for $T_e = T_{\text{ph}}$. Then electron temperature during any moment of relaxation is $T_e = T_{\text{ph}} + \Delta T_e = T_{\text{ph}} + (-\delta P/\delta I_{\text{test}} \times dI_{\text{sw}}/dT_e)^{-1}\Delta P$. The conversion formula is the result of mutual relation (i.e., triple product rule) between three partial derivatives $\delta P/\delta I_{\text{test}}$, $\delta I_{\text{test}}/\delta T_e$, $\delta P/\delta T_e$ illustrated in Fig. 2(e). Collection of $P(I_{\text{test}})$ dependences at different temperatures gives knowledge of $\delta P/\delta I_{\text{test}}$ and dI_{sw}/dT_e, and allows us to calculate the temperature responsivity at constant testing current amplitude $(\Delta P/\Delta T_e)_{I_{\text{test}}}$. The uncertainty in T_e determination is set by accuracy of probability measurement [34], that is $\Delta P_{\text{un}} = [P(1-P)/N]^{1/2}$ (N is number of pulses) and reads $\Delta T_{e,\text{un}} = (-\delta P/\delta I_{\text{test}} \times dI_{\text{sw}}/dT_e)^{-1}\Delta P_{\text{un}}$. The method is applicable only for linear regime when $\Delta P \sim \Delta T_e$. We define a NET in units of $\text{K}/\sqrt{N}$ as the normalized uncertainty $\Delta T_{e,\text{un}} \times \sqrt{N}$ [see Fig. 2(f), right axis]. Increasing number of testing pulses is equivalent to reduction of the measurement bandwidth.

B. Temperature from switching current

The second method of temperature determination requires only knowledge of the $I_{\text{sw}}(T_e, P = P_{\text{goal}})$ curve. Here, during the relaxation process, the bisection algorithm iteratively finds the switching current corresponding to probability $P = P_{\text{goal}} \pm \Delta P_{\text{bis}}$ (the search is stopped when measurement yields the probability from the specified interval). The obtained value is converted into temperature. The uncertainty in T_e determination is set by accuracy of probability measurement, like in the first method, but in addition it also suffers from nonzero value of ΔP_{bis}, which for typical experiment is $\Delta P_{\text{bis}} = 0.01 - 0.02$, significantly bigger than ΔP_{un}. We get for the second method $\Delta T_{e,\text{un}} = (-\delta P/\delta I_{\text{test}} \times dI_{\text{sw}}/dT_e)^{-1} \times (\Delta P_{\text{un}} + \Delta P_{\text{bis}})$. The method is less sensitive but it is well suited for probing transients in a nonlinear regime.

IV. QP DIFFUSION MEASUREMENT

To trace propagation of hot electrons, we first create their population applying short current pulse (with nominal length 10 ns) to the copper island (ports 1 and 2 in Fig. 1) and then we send the testing pulse on the bridge (ports 1 and 3 in Fig. 1). The testing pulse consists of two parts: probing section–nominally 10 ns long, followed by a few μs sustain part needed for readout of the state of the junction [16]. We repeat the whole sequence N times to measure switching probability corresponding to the given delay between the two pulses. The delay can be set with accuracy better than 1 ns. Varying the delay allows us to reconstruct the temporal variation of the switching probability as the electron diffusion proceeds. The temporal resolution of the measurement is limited by the length of the probing portion of the testing pulse: the bridge can switch only for the topmost part of the pulse, which is estimated to be approximately 6 ns in our experiment (see Appendix A). It accounts for the relative accuracy of the delay equal to the half of the width of the testing pulse, i.e., ± 3 ns.

The typical experimental profile is presented in Fig. 3. The hot-electron signal peaks up approximately 300 ns after application of nominally 10-ns-long heating pulse,

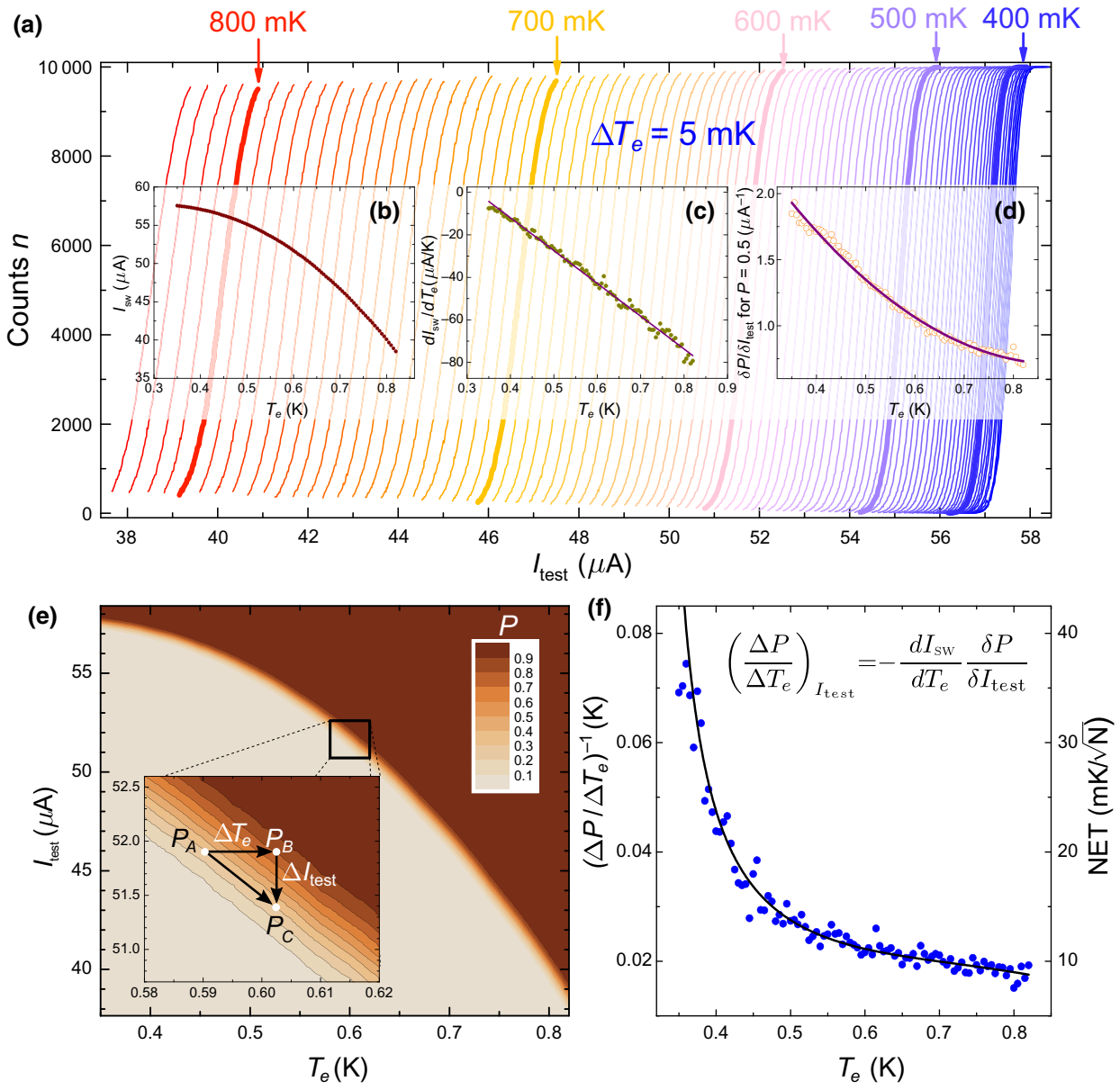

FIG. 2. Switching thermometry. (a) Main panel presents collection of S curves recorded at various bath temperatures with $N = 10\,000$. (b) Temperature dependence of the switching current $I_{sw} = I_{test}(P = 0.5)$ as extracted from the S curves. The dependence serves as the calibration curve in the "Temperature from switching current" method (see discussion in the text). (c) Switching current responsivity dI_{sw}/dT_e. (d) Slope of the S curves $\delta P/\delta I_{test}$. (e) Experimental dependence of the switching probability P on the testing current I_{test} and temperature T_e. The map is different presentation of S curves displayed in (a). Inset: close up of the dependence with indicated probabilities P_A, P_B, and $P_C = P_A$. The zero change in probability on the path ABC ($\Delta P_{ABC} = \Delta P_{AB} + \Delta P_{BC} = 0$) allows us to establish temperature responsivity $\Delta P/\Delta T_e$. (f) $(\Delta P/\Delta T_e)^{-1}$ serving as the calibration curve in the "Temperature from probability" method (left axis) and the resulting NET (right axis). The lines imposed on the experimental data are empirical polynomial fits.

which qualitatively agrees with diffusion time across 60-μm-long nanowire, discussed earlier. One can observe the delay of approximately 40 ns between the heating pulse and the onset of the signal. Importantly, the delay shows that switching current of the bridge depends on the local distribution (local temperature) of QPs, not on the temperature of the electromagnetic environment (see also Secs. VI and VII). The experimental profile allows us to determine the diffusion constant via direct comparison with simple free-particle diffusion model (Fig. 3, see also Supplemental Material [30]). The fit yields value of $D = (100 \pm 5)$ cm^2/s. Since the diffusion constant, governing the spreading of electrons in one particular direction (i.e., along the length of the wire), is equal to

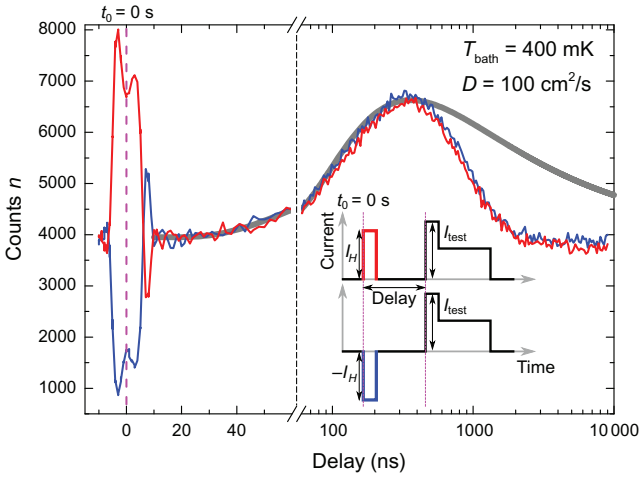

FIG. 3. Switching probability as a function of delay between heating (red or blue, I_H applied between ports 1 and 2) and testing pulse (black, I_{test} applied between ports 1 and 3). Two traces are imposed on each other corresponding to two current polarities of the heating pulse. The delay equal 0 corresponds to the testing and heating pulse arriving to the device at the same time. In such a case, a small fraction of the heating pulse ($< 0.5\%$) flows through the bridge, subtracting from or adding to the testing pulse. The temporal overlap of the heating and testing pulse is therefore well visible in the switching probability offering a convenient mean for timing calibration of the experiment. Noteworthy, two heating pulses of different polarities, but of the same amplitude, produce the same thermal response, as expected. The number of pulses to measure each point is $N = 10\,000$ with repetition time of 100 μs. The thick solid line is the simple free-particle diffusion model presented in Fig. 1 fitted to the onset of the signal for $D = 100$ cm^2/s. The vertical line cuts the timescale into a linear and a logarithmic part.

$D = 1/3 \times v_F \times l_{\mathrm{MFP}}$, setting $v_F = 2 \times 10^6$ m/s we obtain $l_{\mathrm{MFP}} = 15$ nm, a value comparable with the grain size of our polycrystalline aluminum (Fig. 1, [30]). Using calibration dependence $(\Delta P/\Delta T_e)^{-1}$ [Fig. 2(f)], we convert the measured signal into electron temperature. In Fig. 4 we present results of such a conversion for different bath temperatures and heating currents. We also heat the copper island with pulses of different duration observing gradual buildup of the temperature profile until the steady state with an elevated temperature on the bridge is reached [Fig. 5(a)]. Similarly, we collect transients appearing after 10-μs-long heating pulse is turned off [Fig. 5(b)].

V. THERMAL MODELING

The onset of the QPs is well described by the free-particle diffusion model, which nevertheless fails to explain the observed signal at longer delays. To understand the overall shape of the experimental diffusion profile we elaborate a more detailed thermal model describing evolution of temperature in the wire. Firstly, owing to enhanced electron-phonon coupling, hot QPs are expected to dissipate their energy to phonons before they reach the bridge. Secondly, diffusing electrons should lose some energy to equilibrate with local and "colder" QPs. We map our three-terminal device into the 1D model to perform simplified heat-flow analysis of the aluminum line interrupted by the 3-μm-long copper section. Instead of considering leads 1 and 2 we replace them with a single lead of the same cross section as lead 3, but with thermal parameters rescaled by a single geometry factor $k = \dot{Q}_1 + \dot{Q}_2/\dot{Q}_3 = 3$ (Fig. 6).

We analyze the diffusion process by numerically solving the one-dimensional time-dependent heat-flow equation for the electron temperature $T_e(x,t)$:

$$\frac{\delta}{\delta x}\left(\kappa\frac{\delta T_e}{\delta x}\right) = C_p\frac{\delta T_e}{\delta t} + \dot{q}_{\mathrm{EP}} - \frac{r \times I_H^2}{S}, \qquad (1)$$

where the left part of the equation describes the net heat flux carried by hot electrons [$\kappa(x,T_e)$ is the electron thermal conductivity] and terms on the right-hand side describe the increase of electron energy [$C_p(x,T_e)$ is electron heat capacity], power transmitted to phonons $\dot{q}_{\mathrm{EP}}(x,T_e)$ and heating defined by a time-dependent current pulse $I_H(t)$. $r(x,T_e)$ is the resistance per unit length and $S = 600$ nm $\times 30$ nm is the cross section of the aluminum nanowire. In solving the equation we assume the literature-based values of thermal parameters [5,30,35,36].

We find the best correspondence between numerical simulation and experimental data assuming the effective resistance of the copper heating island $R_{\mathrm{eff}} = 1.6\ \Omega$. This parameter is used consequently for all modeling. The R_{eff} value is roughly three times smaller than the measured resistance ($R = 4.5\ \Omega$) of the heater line spanning between ports 1 and 2 (see Fig. 1). The difference can be ascribed to the fact that hot electrons created in the copper heater are Andreev reflected at the normal-metal–superconductor interface and only those with sufficiently high energies can enter into the aluminum nanowire as nonequilibrium QPs [37,38]. The calculated temperature profiles are imposed on the experimental data in Figs. 4 and 5.

Fully quantitative analysis based on the heat-flow equation presented in the text gives a good agreement with experimental profiles. Our model uses only one fitting parameter R_{eff} for all profiles, otherwise it is based on thermal parameters available in the literature [30]. Considering their functional dependences the agreement is remarkable. We use the logarithmic scale in Figs. 4 and 5 for the horizontal axis, although it magnifies any discrepancies between the model and experimental data for short delay times. On the other hand, it allows us to perform the comparison over 3 orders of magnitude of the temporal scale. We see that the thermal model reconstructs the timing of the experiment surprisingly good. The model predicts well the time delay for the onset of the signal, the moment of its accumulation (the peak) and delivers

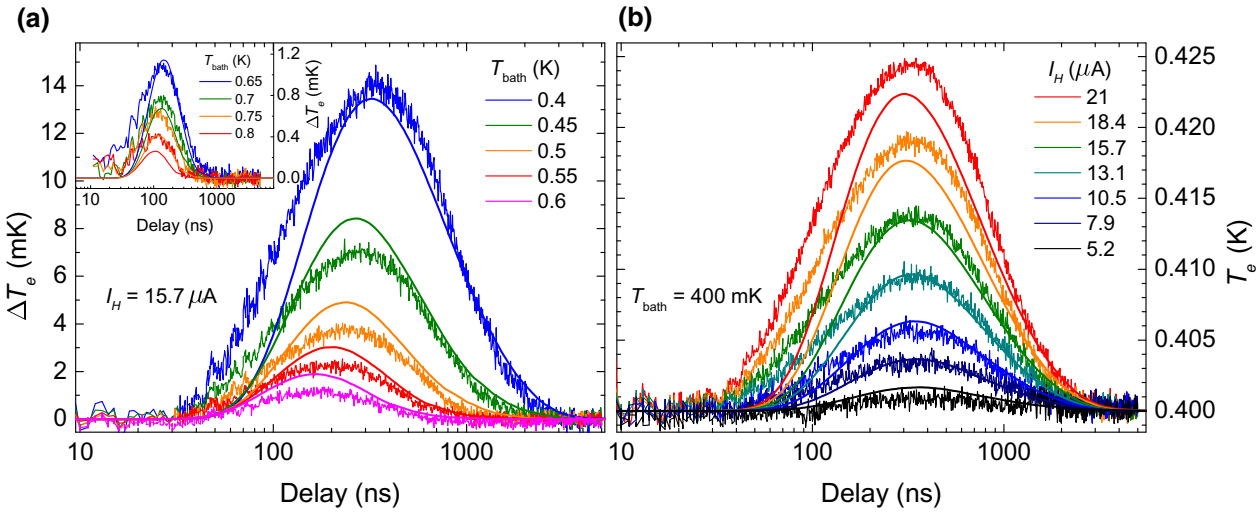

FIG. 4. Temperature dynamics of the superconducting nanobridge after creating nonequilibrium QPs in the copper heater placed 60-μm away with a short heating pulse. (a) Hot-electron signal measured for the same heating pulse at various bath temperatures: 0.4–0.6 K (main panel) and 0.65–0.8 K (inset). Noteworthy, the hot-electron signal for $T = 800$ mK shows only $400-\mu$K peak with accuracy better than 100 μK. (b) Hot-electron signal measured at constant temperature for various heating pulses. The "noisy" profiles are experimental data for which the temperature is extracted with the "temperature from probability" procedure. Solid lines are calculated numerically for the 1D heat-flow model discussed in the text.

proper relaxation time for the tail of the signal. In fact, it proved to be very helpful in designing the geometry of our sample. Our modeling properly captures the suppression of the hot-electron signal with increasing bath temperature (as arising from the enhanced electron-phonon coupling and the larger heat capacity). It also properly describes the effect of the heating power and transients leading to the steady states (see Fig. 5). The model contains no effect of electromagnetic environment.

The measurements presented in Fig. 4 reveal the spatial range of QPs, their lifetime, and identifies mechanisms responsible for their annihilation. We observe the fast buildup (of order of 100 ns) of QPs' population at the detector in response to a remote heating pulse. The signal is much more pronounced at lower temperatures, where electron-phonon coupling is suppressed [30]. At $T_{\rm bath} = 0.4$ K relaxation time is of order of 1 μs and it decreases to approximately 100 ns at $T_{\rm bath} = 0.8$ K owing to the dominant role of electron-phonon coupling on electron temperature relaxation at higher temperatures.

VI. THE EXPERIMENTAL FACT FOR THE LACK OF INFLUENCE OF ELECTROMAGNETIC ENVIRONMENT ON THE MEASURED EXPERIMENTAL PROFILES

It may come as a surprise that our results are not affected by electromagnetic environment of the junction, as expected from the orthodox theory of the thermally activated switching [39]. We observe the delay of approximately 40 ns between the heating pulse and the onset of the signal on the bridge (Figs. 3 and 4). Heating pulse heats up the different parts of the junction environment. Generally, one can expect that the change of temperature of electromagnetic environment should be immediately seen on the bridge, since electromagnetic signals propagate at the speed of light. Moreover, the biggest signal should be seen on the bridge just after heating pulse is over, when the environment is at the highest elevated temperature. It is not the case in our experiment. After we send pulse on the heater line, there are no response on the bridge for a few dozens of nanoseconds. It proves that the measured profile (Fig. 3) is not sensitive to changes in temperature of the remote electromagnetic environment of the bridge as it is also confirmed in Sec. VII and Appendix A. The circuit analysis (see Appendix B) shows that the Johnson-Nyquist noise of the heater is shorted to ground and cannot affect the switching process. On the other hand, the noise generated on the testing line does not change during switching measurements and creates a constant background for the signal without affecting the diffusion profiles of quasiparticles.

VII. EQUIVALENCE OF THE STATIC AND DYNAMIC TEMPERATURE

We measure a set of S curves during the temporal transient. The results are presented in Fig. 7. The *dynamic* S *curves* look exactly the same as the *static* S *curves* collected in the equilibrium state, further proving that the switching in our case is only sensitive to the local distribution of quasiparticles, not to the environmental noise. It allows us to translate the time dependence of probability

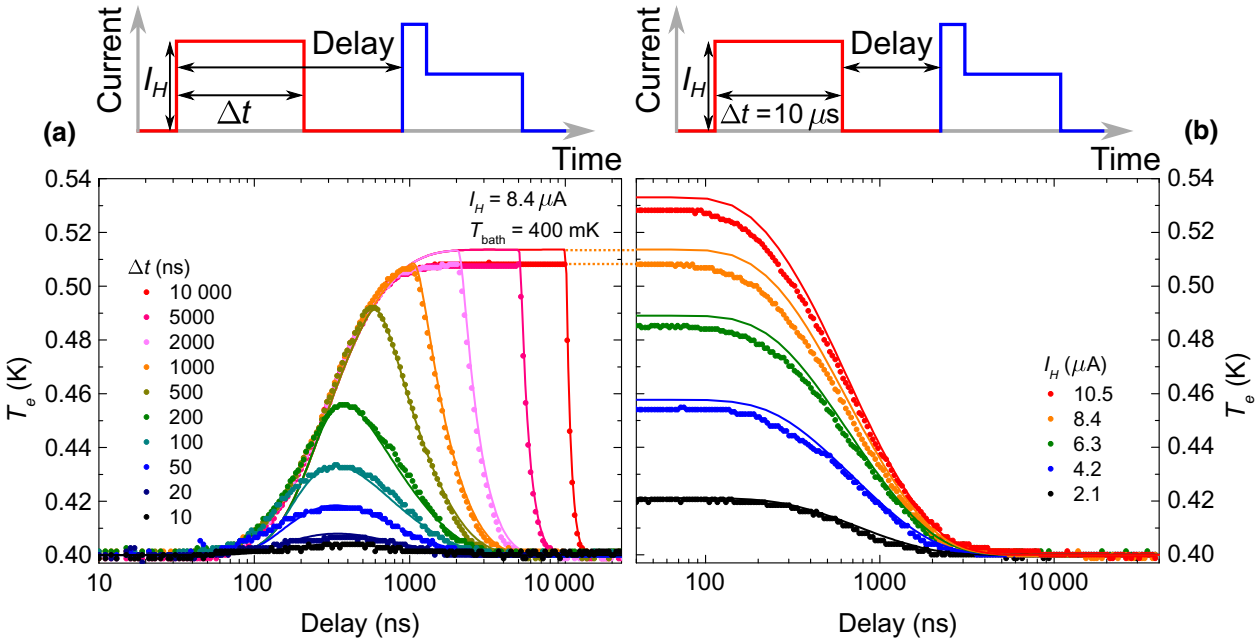

FIG. 5. Temperature dynamics of the superconducting nanobridge after creating nonequilibrium QPs in the copper heater placed 60-μm away with a long heating pulse. (a) Hot-electron signal measured for heating pulses of the various duration and the same amplitude ($I_H = 8.4\ \mu$A). (b) Hot-electron signal measured for heating pulses of the various amplitude and the same duration ($\Delta t = 10\ \mu$s). The definition of measurement is depicted above each figure. The "dotted" profiles are experimental data for which the temperature is extracted with the "temperature from switching current" procedure. Solid lines are calculated numerically for the 1D heat-flow model discussed in the text.

into the time dependence of temperature with the aim of the static calibration.

VIII. DISCUSSION

One can expect that at higher bath temperatures, owing to higher average energy QPs should arrive to the detector faster. Such an expectation is a result of group velocity v_g scaling with energy as $v_g = v_F\sqrt{1-\Delta^2/E^2}$, where Δ is the superconducting gap [4]. It is not what we see in the experiment. The temporal onset of the signal does not depend on temperature and heating power. Instead, all profiles for short delays can be fitted with the same diffusion constant [30].

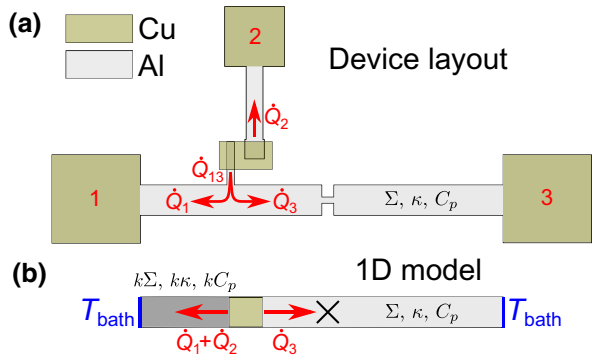

FIG. 6. (a) Layout of the nanostructure. (b) The modeled 1D strip with left-hand-side thermal parameters modified to account for the heat-flow asymmetry in the real structure. Based on similar surfaces of NS interfaces defined on the top of the copper island (see inset of Fig. 1) we assume that total generated heat gives rise to two equal heat fluxes $\dot{Q}_2$ and $\dot{Q}_{13}$ ($\dot{Q}_2 = \dot{Q}_{13} = \dot{Q}_1 + \dot{Q}_3$ and $\dot{Q}_1 = \dot{Q}_3$) responsible for evacuation of the energy from the heater.

The long lifetime and spatial range of QPs at low temperatures make it obligatory to engineer gap and trap structures for single-electron boxes [40,41], microcoolers [42], and qubits [43]. The presented experiment can be easily modified to test the efficacy of QP trapping in normal metal [44–46], or in Meissner or vortex states [41], if a normal-metal island or a wider piece of aluminum strip (allowing to accommodate a vortex [47]) is inserted on the way between the heater and the detector.

We measure QPs' propagation down to 400 mK. The lifetime and propagation range are expected to be vastly increased when lowering temperature towards absolute zero. The natural extension of the current work is a measurement of QP diffusion at temperatures below 100 mK, typical for superconducting qubit operation. It can be accomplished by using Josephson junction exhibiting switching-current sensitivity at lower temperatures compared to the presented aluminum nanobridge. An *S-N-S* proximity junction or a titanium nanobridge would perhaps be good candidates. Studies at the lowest temperatures can

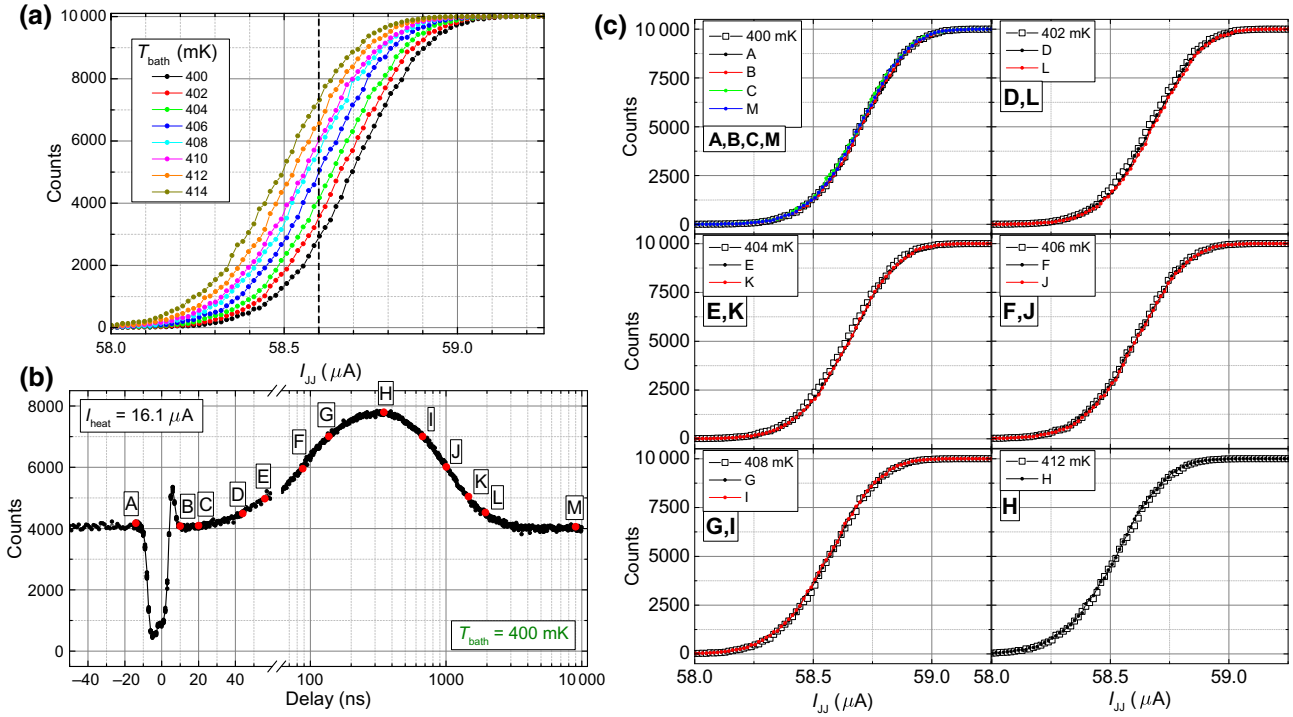

FIG. 7. Comparison of the S curves collected in the static and dynamic measurements. (a) Set of the static S curves collected at the fixed bath temperatures (in the equilibrium state). (b) Dependence of the switching probability on the delay between heating and testing pulse. (c) The dynamic S curves (solid circles) collected for various delays corresponding to points A, B,. . ., M in (b) as compared to the static S curves measured at fixed bath temperatures (open squares). Since our S curves (points B and C) do not detect the effect of the heating pulse for the first approximately 25 ns (they look exactly the same as the S curve measured in equilibrium without application of the heating pulse), we conclude that environmental effects have negligible influence on the changes in the measured signal after application of the heating pulse.

help to resolve the mystery of the residual QP density, which appears not to follow the BCS theory.

The BCS value of coherence length ξ_{BCS} for aluminum in the clean limit ($l_{MFP} \gg \xi_{BCS}$) is ξ_{BCS}=1.6 μm. In our case, $l_{MFP} = 15$ nm and the coherence length is rescaled to be $\xi = 0.85(\xi_{BCS} \times l_{MFP})^{0.5} = 132$ nm. Our nanobridge has a length of $l = 230$ nm. For a superconducting nanobridge to be a Josephson junction understood as a set of Andreev bound states, we require $l < \xi$. Our bridge does not satisfy this criterion and perhaps comprises an element in between a Josephson junction and a short wire. We note, however, that it is not essential in the current presentation, which utilizes the bridge as a tool to get insight into thermal dynamics of the superconducting nanostructure, and does not focus on the description of the switching mechanism of the bridge.

We emphasis that the interpretation of our experiment does not depend on the switching mechanism. We rely on the calibration of the switching probability against the bath temperature. Such an approach is the only possible way to interpret the switching current in terms of the physical temperature. We notice that theories describing the escape mechanism hardly have the predictive character in quantitative terms. They are used in the physics of Josephson junctions (JJs) and nanowires to explain the shape of the observed switching histograms and S curves but applied alone they cannot be used to find the thermodynamic temperature of the experiment. In general, the extraction of the thermodynamic temperature is only possible if the escape process is governed solely by thermal fluctuations. Even then, great care must be taken to interpret the data properly, for there is the double-exponential dependence involved in calculations of the switching probability with some parameters poorly known.

Variations of switching current in JJs are set by two factors: (i) value of the superconducting gap (it is local property of the junction that together with temperature sets its critical current according to the Ambegaokar-Baratoff formula) and (ii) strength of electromagnetic fluctuations induced by environment (it is a nonlocal property that may make the junction sensitive to temperature of remote impedance). In the case of a Dayem nanobridge with critical current of about 50 μA, as the one studied here, the first factor dominates and fluctuations play a minor role: switching current follows closely the critical current temperature dependence [30]. Since I_C is the local property of the bridge, its measurement reflects the temperature of the bridge. It is in contrast to a tunnel junction (with

$I_C < 1\,\mu$A) for which the switching current is significantly suppressed compared to I_C due to electromagnetic fluctuations of the environment [30,39,48].

IX. CONCLUSIONS

We demonstrate the real-time measurement of the nonequilibrium QP diffusion in the superconducting aluminum nanowire. Such an investigation is possible because our fast thermometry delivers resolution at single-nanosecond level ($t_{\rm res} \sim 1$ ns) accessing the regime where $t_{\rm res} \ll L^2/D$ with L being the spatial extent of the experiment (i.e., distance between QP source and detector). Our data are in agreement both with the simple model of the free-particle diffusion (allowing for direct determination of the diffusion constant), and a more involved thermal model taking into consideration the electron-electron and electron-phonon scatterings with the first mechanism being accounted for by the electron heat capacity term and the second one by electron-phonon coupling in the heat-flow equation. Curiously enough, the method involves measurement of somewhat abstract probability from which electron temperature can be obtained. The presented switching thermometry allows us to study fast nonequilibrium thermal processes in nanostructures offering an attractive tool for experimental quantum thermodynamics and caloritronics.

ACKNOWLEDGMENTS

The authors thank Olli-Pentti Saira and Denis Vodolazov for helpful discussions and Paulina Grzaczkowska for technical support. The work is financed by Foundation for Polish Science (First TEAM/2016-1/10).

APPENDIX A: ON-CHIP IMAGING OF THE TESTING PULSE

The square pulses in Fig. 3 correspond to their nominal definition in the 80-MHz generator and is presented for conceptual purpose, mainly intended to explain the timing of the experiment. In fact, our 80-MHz generator delivers pulses with leading and trailing edges of 3 ns. The real shape of the testing pulse, as recorded on the 600 MHz (2 GS/sec) oscilloscope, is presented in Fig. 8.The bridge can switch only for the topmost part of the pulse in the current interval qualitatively corresponding to the S-curve width. The testing time is thus approximately 6 ns.

One may wonder if the actual probing and heating pulse reach the nanodevice with its shape unperturbed. To control the quality of the pulse reaching the sample we scan the testing pulse over the pilot pulse varying the time delay between them (Fig. 9). Both pulses are sent on the same line. The pilot pulse has much lower amplitude, but it contains no sustain part. When two pulses arrive to the bridge at the same time we observe enhancement of the switching probability and verify the actual duration and shape

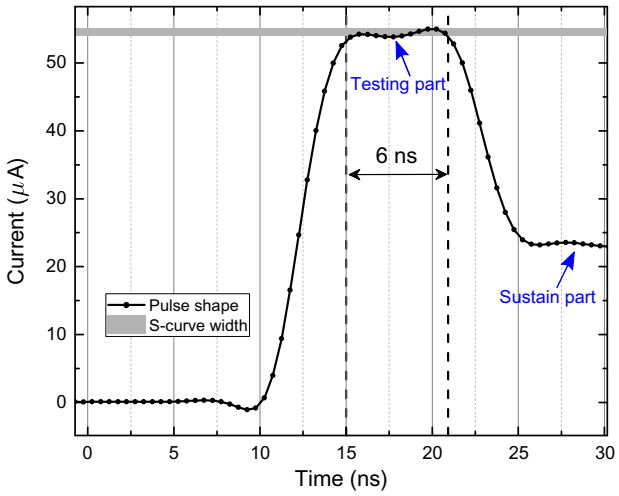

FIG. 8. The oscilloscope trace of the nominally 10-ns-long testing pulse used in the experiment presented in the main text. The testing time is approximately 6 ns. It is followed by the long sustain part (approximately 5 μs) necessary for the readout of the switching event (Fig. 3 in Ref. [16]).

of the testing pulse. The obtained image confirms that the pulse reaching the bridge arrives unperturbed preserving its nominal leading and trailing edges. What we observe is a convoluted image of the pulse since the testing pulse cannot be made infinitely short. A similar image of the testing pulse is presented in Fig. 3 for delays around zero. In that case, a small fraction of the heating pulse ($< 0.5\%$) travels to the bridge playing the role of the pilot pulse and modifies the switching probability. This modification can be positive or negative, depending on the polarity of the heating pulse. The pilot pulse response does not exhibit any unexpected features, which could potentially resemble the diffusive profile observed in the main experiment, i.e., there is no enhancement of the measuring probability for times where two pulses do not overlap. It gives yet another strong support to our interpretation of the experiment ruling out electromagnetic environment effects on the measured diffusive profiles.

APPENDIX B: NOISE ANALYSIS OF THE ELECTROMAGNETIC ENVIRONMENT

The equivalent circuit with the environmental sources of Johnson-Nyquist noise is presented in Fig. 10. It contains two bias resistors: $R_{\rm BT}$ on the line probing the switching probability of the bridge and $R_{\rm BH}$ on the heating line. In addition there is a resistor $R_{\rm heater}$ describing the heater. Each of resistors has its own effective temperature and is a source of the Johnson-Nyquist noise. There are three such sources depicted in Fig. 10: $i_{\rm NH}$, $i_{\rm NBH}$, $i_{\rm NBT}$. The current noise produced by $i_{\rm NH}$ and $i_{\rm NBH}$ sources is not visible on the bridge as it is shorted to ground. It is true for any

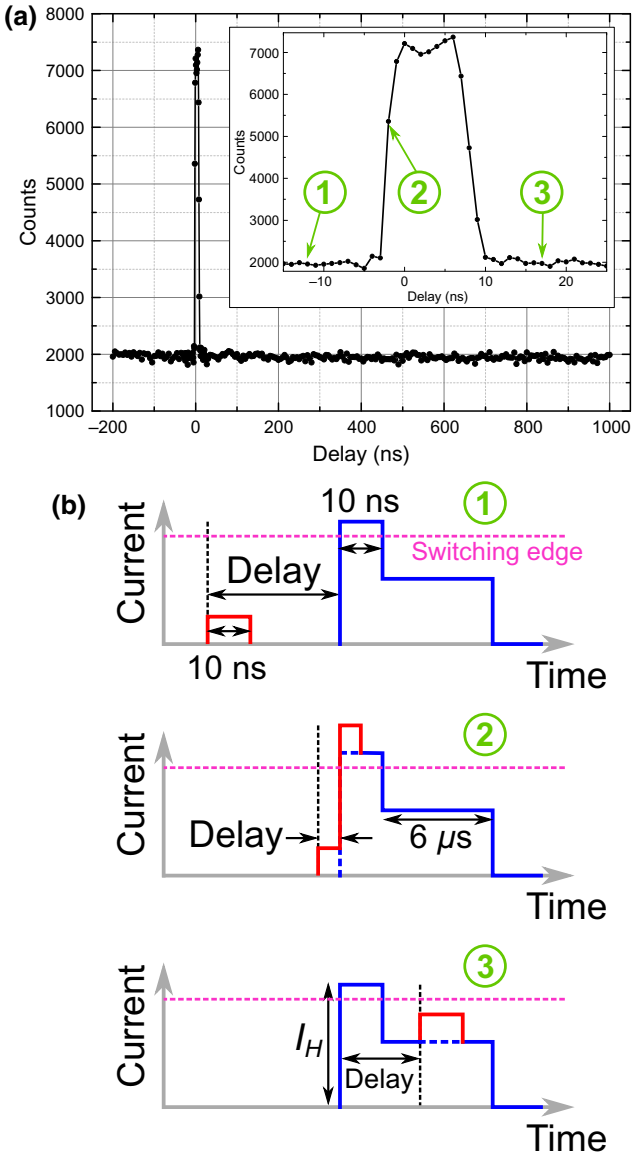

FIG. 9. (a) The "on-chip image" of the testing pulse. The inset presents the enlarged signal. (b) The testing pulse (blue pulse) is delayed with respect to the pilot pulse (red pulse). When two pulses overlap the enhancement in the switching probability is observed (state 2). The pilot pulse has the same definition as the testing pulse (without the sustain part) but much smaller amplitude. The shape of the probing pulse is presented in Fig. 8. The pilot pulse does not influence the measured signal outside the temporal window, where the two pulses do not overlap.

effective temperature of resistors R_{BH} and R_{heater}? Electromagnetic noise produced by resistors R_{BH} and R_{heater} cannot influence the switching of the bridge. The bridge is only sensitive to the effective temperature of the resistor R_{BT}. This temperature does not change during probing the relaxation and as such, cannot be responsible for changing the probability. It leads us to the conclusion that the only possible source of probability changes on the bridge is

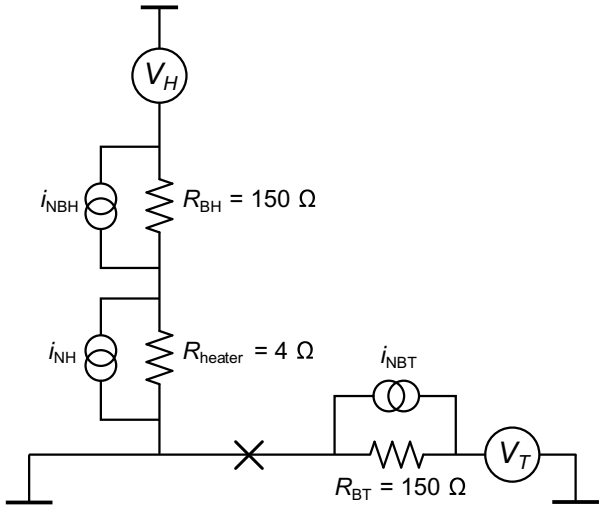

FIG. 10. The equivalent current noise circuit of the full experimental setup. The noise from i_{NH} and i_{NBH} sources is shorted to ground and cannot affect switching probability of the bridge.

local temperature (local distribution of the quasiparticles). The actual electrical circuit probing the bridge is presented within the Supplemental Material [30].

APPENDIX C: CAN PHONON EMISSION CHANNEL BE RESPONSIBLE FOR THE OBSERVED SIGNAL?

At low temperatures electrons and phonon systems are decoupled thermally from each other and generally we talk about two temperatures: electron temperature and lattice temperature. Our bridge measures electron temperature and is not sensitive to phonon temperature. Once electrons are heated above the lattice temperature they start to give up energy to phonons. This energy relaxation channel is often referred to as electron-phonon coupling. At ultralow temperatures (< 1 mK) it can take hours for both systems to equilibrate. For our moderately low temperatures (approximately 400 mK) the process of equilibration takes roughly 1–10 μs [2,16]. This time can be inferred from the relaxation tails of the diffusive profiles presented in Fig. 4, when the temperature profile along wire is already flat (meaning that temperature gradients in the wire are small) and the electron temperature relaxation proceeds through the electron-phonon channel predominantly. In the Supplemental Material [30] we present also the difference in the measured profiles if electron-phonon relaxation channel did not exist. One may easily see that the result is almost unaltered at 400 mK. Diffusing electrons reach the bridge after approximately 40 ns. This time is much too short for electron-phonon coupling to act: electrons reach the bridge before they get a chance to sink their excess energy to phonons. For larger time delays phonons get some energy from electrons, which in turn they sink in the substrate

(here one talks about thermal Kapitza resistance between the sample and substrate). It is usually assumed for steady-state measurements that this interaction allows phonons in the sample to remain well thermalized at bath temperature [49,50]. We use very short heating pulse so that the amount of deposited energy is much smaller than during steady-state investigations and should not lead to overheating of the phonons. Even if phonons are slightly overheated the energy flux from electrons to phonons hardly changes owing to strong power-law dependence [30].

To consider substrate phonons as being responsible for the measured diffusive profiles we need to assume the following processes: electron-phonon coupling in the sample, phonon-phonon coupling across the sample-substrate interface, propagation of phonons in the substrate, phonon-phonon coupling across substrate-sample interface, heating electrons with sample phonons. Moreover, propagation of phonons in the substrate needs to be ballistic because our signal propagates with speed of the running acoustic wave ($V \approx 60\ \mu\text{m}/40\ \text{ns} = 1500\ \text{m/s}$; 60 μm is the on-chip distance between heater and the bridge, 40 ns is the delay between heating time and the onset of the signal on the bridge). Additionally, we need to assume surface phonon. Such a ballistic surface phonon needs to excite the phonon in the sample in the locus of the bridge or excite the electron in the nanowire directly. Only electrons with an excess energy can be detected with our thermometer. We think such a process has very low probability and can carry negligible amount of energy. We conclude that substrate phonons cannot be responsible for the measured signal.

[1] F. C. Wellstood, C. Urbina, and John Clarke, Hot-electron effects in metals, Phys. Rev. B **49**, 5942 (1994).

[2] A. V. Timofeev, C. Pascual García, N. B. Kopnin, A. M. Savin, M. Meschke, F. Giazotto, and J. P. Pekola, Recombination-Limited Energy Relaxation in a Bardeen-Cooper-Schrieffer Superconductor, Phys. Rev. Lett. **102**, 017003 (2009).

[3] M. Meschke, W. Guichard, and J. P. Pekola, Single-mode heat conduction by photons, Nature **444**, 187 (2006).

[4] J. N. Ullom, P. A. Fisher, and M. Nahum, Energy-dependent quasiparticle group velocity in a superconductor, Phys. Rev. B **58**, 8225 (1998).

[5] H. Courtois, M. Meschke, J. T. Peltonen, and J. P. Pekola, Origin of Hysteresis in a Proximity Josephson Junction, Phys. Rev. Lett. **101**, 067002 (2008).

[6] Francesco Giazotto and María José Martínez-Pérez, The Josephson heat interferometer, Nature **492**, 401 (2012).

[7] S. Jezouin, F. D. Parmentier, A. Anthore, U. Gennser, A. Cavanna, Y. Jin, and F. Pierre, Quantum limit of heat flow across a single electronic channel, Science **342**, 601 (2013).

[8] S. Gasparinetti, F. Deon, G. Biasiol, L. Sorba, F. Beltram, F. Giazotto, and 'Probing the local temperature of a two-dimensional electron gas microdomain with a quantum dot, Measurement of electron-phonon interaction, Phys. Rev. B **83**, 201306 (2011).

[9] A. C. Betz, F. Vialla, D. Brunel, C. Voisin, M. Picher, A. Cavanna, A. Madouri, G. Fève, J.-M. Berroir, B. Plaçais, and E. Pallecchi, Hot Electron Cooling by Acoustic Phonons in Graphene, Phys. Rev. Lett. **109**, 056805 (2012).

[10] B. Michon, A. Ataei, P. Bourgeois-Hope, C. Collignon, S. Y. Li, S. Badoux, A. Gourgout, F. Laliberté, J.-S. Zhou, Nicolas Doiron-Leyraud, and Louis Taillefer, Wiedemann-Franz law and Abrupt Change in Conductivity across the Pseudogap Critical Point of a Cuprate Superconductor, Phys. Rev. X **8**, 041010 (2018).

[11] D. R. Schmidt, C. S. Yung, and A. N. Cleland, Temporal measurement of hot-electron relaxation in a phonon-cooled metal island, Phys. Rev. B **69**, 140301 (2004).

[12] O.-P. Saira, M. Zgirski, K. L. Viisanen, D. S. Golubev, and J. P. Pekola, Dispersive Thermometry with a Josephson Junction Coupled to a Resonator, Phys. Rev. Appl. **6**, 024005 (2016).

[13] S. Gasparinetti, K. L. Viisanen, O.-P. Saira, T. Faivre, M. Arzeo, M. Meschke, and J. P. Pekola, Fast Electron Thermometry for Ultrasensitive Calorimetric Detection, Phys. Rev. Appl. **3**, 014007 (2015).

[14] R. Barends, J. J. A. Baselmans, S. J. C. Yates, J. R. Gao, J. N. Hovenier, and T. M. Klapwijk, Quasiparticle Relaxation in Optically Excited High-q Superconducting Resonators, Phys. Rev. Lett. **100**, 257002 (2008).

[15] K. L. Viisanen and J. P. Pekola, Anomalous electronic heat capacity of copper nanowires at sub-kelvin temperatures, Phys. Rev. B **97**, 115422 (2018).

[16] M. Zgirski, M. Foltyn, A. Savin, K. Norowski, M. Meschke, and J. Pekola, Nanosecond Thermometry with Josephson Junctions, Phys. Rev. Appl. **10**, 044068 (2018).

[17] Jian Wei, David Olaya, Boris S. Karasik, Sergey V. Pereverzev, Andrei V. Sergeev, and Michael E. Gershenson, Ultrasensitive hot-electron nanobolometers for terahertz astrophysics, Nat. Nanotechnol. **3**, 496 (2008).

[18] J. Govenius, R. E. Lake, K. Y. Tan, and M. Möttönen, Detection of Zeptojoule Microwave Pulses Using Electrothermal Feedback in Proximity-Induced Josephson Junctions, Phys. Rev. Lett. **117**, 030802 (2016).

[19] Evan D. Walsh, Dmitri K. Efetov, Gil-Ho Lee, Mikkel Heuck, Jesse Crossno, Thomas A. Ohki, Philip Kim, Dirk Englund, and Kin Chung Fong, Graphene-Based Josephson-Junction Single-Photon Detector, Phys. Rev. Appl. **8**, 024022 (2017).

[20] Francesco Giazotto, Tero T. Heikkilä, Arttu Luukanen, Alexander M. Savin, and Jukka P. Pekola, Opportunities, for mesoscopics in thermometry and refrigeration, Rev. Mod. Phys. **78**, 217 (2006).

[21] K. Serniak, M. Hays, G. de Lange, S. Diamond, S. Shankar, L. D. Burkhart, L. Frunzio, M. Houzet, and M. H. Devoret, Hot Nonequilibrium Quasiparticles in Transmon Qubits, Phys. Rev. Lett. **121**, 157701 (2018).

[22] Diego Rainis and Daniel Loss, Majorana qubit decoherence by quasiparticle poisoning, Phys. Rev. B **85**, 174533 (2012).

[23] David Aasen, Michael Hell, Ryan V. Mishmash, Andrew Higginbotham, Jeroen Danon, Martin Leijnse, Thomas S. Jespersen, Joshua A. Folk, Charles M. Marcus, Karsten Flensberg, and Jason Alicea, Milestones toward

Majorana-Based Quantum Computing, Phys. Rev. X **6**, 031016 (2016).

[24] Jukka P. Pekola, Towards quantum thermodynamics in electronic circuits, Nat. Phys. **11**, 118 (2015).

[25] Antonio Fornieri and Francesco Giazotto, Towards phase-coherent caloritronics in superconducting circuits, Nat. Nanotechnol. **12**, 944 (2017).

[26] Antonio Fornieri, Giuliano Timossi, Pauli Virtanen, Paolo Solinas, and Francesco Giazotto, 0-π phase-controllable thermal Josephson junction, Nat. Nanotechnol. **12**, 425 (2017).

[27] M. J. Martínez-Pérez, P. Solinas, and F. Giazotto, Coherent caloritronics in Josephson-based nanocircuits, J. Low Temp. Phys. **175**, 813 (2014).

[28] Nianbei Li Jie Ren, Lei Wang, Gang Zhang, Peter Hänggi, and Baowen Li 'Colloquium, Phononics: Manipulating heat flow with electronic analogs and beyond, Rev. Mod. Phys. **84**, 1045 (2012).

[29] Gerrit E. W. Bauer, Eiji Saitoh, and Bart J. van Wees, Spin caloritronics, Nat. Mater **11**, 391 (2012).

[30] See Supplemental Material at http://link.aps.org/supplemental/10.1103/PhysRevApplied.14.044024 for sample fabrication, experimental setup, influence of the electron-phonon interaction on the quasiparticle diffusion, diffusion constant for various temperatures and different heating power, numerical calculations and material parameters, note on the effect of the electromagnetic environment on the switching probability, a note on the free-particle diffusion model versus the heat-flow equation.

[31] M. L. Roukes, M. R. Freeman, R. S. Germain, R. C. Richardson, and M. B. Ketchen, Hot Electrons and Energy Transport in Metals at Millikelvin Temperatures, Phys. Rev. Lett. **55**, 422 (1985).

[32] M. E. Gershenson, D. Gong, T. Sato, B. S. Karasik, and A. V. Sergeev, Millisecond electron-phonon relaxation in ultrathin disordered metal films at millikelvin temperatures, Appl. Phys. Lett. **79**, 2049 (2001).

[33] B. Huard, H. Pothier, D. Esteve, and K. E. Nagaev, Electron heating in metallic resistors at sub-kelvin temperature, Phys. Rev. B **76**, 165426 (2007).

[34] M. Zgirski, M. Foltyn, A. Savin, and K. Norowski, Flipping-Coin Experiment to Study Switching in Josephson Junctions and Superconducting Wires, Phys. Rev. Appl. **11**, 054070 (2019).

[35] V. F. Maisi, S. V. Lotkhov, A. Kemppinen, A. Heimes, J. T. Muhonen, and J. P. Pekola, Excitation of Single Quasiparticles in a Small Superconducting Al Island Connected to Normal-Metal Leads by Tunnel Junctions, Phys. Rev. Lett. **111**, 147001 (2013).

[36] Norman E. Phillips, Heat capacity of aluminum between 0.1°k and 4.0°k, Phys. Rev. **114**, 676 (1959).

[37] E. V. Bezuglyi and V. Vinokur, Heat Transport in Proximity Structures, Phys. Rev. Lett. **91**, 137002 (2003).

[38] Jonghwa Eom, Chen-Jung Chien, and Venkat Chandrasekhar, Phase Dependent Thermopower in Andreev Interferometers, Phys. Rev. Lett. **81**, 437 (1998).

[39] John M. Martinis, Michel H. Devoret, and John Clarke, Experimental, tests for the quantum behavior of a macroscopic degree of freedom: The phase difference across a Josephson junction, Phys. Rev. B **35**, 4682 (1987).

[40] J. Aumentado, Mark W. Keller, John M. Martinis, and M. H. Devoret, Nonequilibrium Quasiparticles and 2*e* Periodicity in single-Cooper-Pair Transistors, Phys. Rev. Lett. **92**, 066802 (2004).

[41] M. Taupin, I. M. Khaymovich, M. Meschke, A. S. Mel'nikov, and J. P. Pekola, Tunable quasiparticle trapping in Meissner and vortex states of mesoscopic superconductors, Nat. Commun. **7**, 10977 (2016).

[42] J. P. Pekola, D. V. Anghel, T. I. Suppula, J. K. Suoknuuti, A. J. Manninen, and M. Manninen, Trapping of quasiparticles of a nonequilibrium superconductor, Appl. Phys. Lett. **76**, 2782 (2000).

[43] John M. Martinis, M. Ansmann, and J. Aumentado, Energy Decay in Superconducting Josephson-Junction Qubits from Nonequilibrium Quasiparticle Excitations, Phys. Rev. Lett. **103**, 097002 (2009).

[44] J. N. Ullom, P. A. Fisher, and M. Nahum, Measurements of quasiparticle thermalization in a normal metal, Phys. Rev. B **61**, 14839 (2000).

[45] R.-P. Riwar, A. Hosseinkhani, L. D. Burkhart, Y. Y. Gao, R. J. Schoelkopf, L. I. Glazman, and G. Catelani, Normal-metal quasiparticle traps for superconducting qubits, Phys. Rev. B **94**, 104516 (2016).

[46] Sukumar Rajauria, L. M. A. Pascal, Ph. Gandit, F. W. J. Hekking, B. Pannetier, and H. Courtois, Efficiency of quasiparticle evacuation in superconducting devices, Phys. Rev. B **85**, 020505 (2012).

[47] Gheorghe Stan, Stuart B. Field, and John M. Martinis, Critical Field for Complete Vortex Expulsion from Narrow Superconducting Strips, Phys. Rev. Lett. **92**, 097003 (2004).

[48] Marek Foltyn and Maciej Zgirski, Gambling with Superconducting Fluctuations, Phys. Rev. Appl. **4**, 024002 (2015).

[49] E. T. Swartz and R. O. Pohl, Thermal boundary resistance, Rev. Mod. Phys. **61**, 605 (1989).

[50] T. Elo, P. Lahteenmaki, D. Golubev, A. Savin, K. Arutyunov, and P. Hakonen, Thermal relaxation in titanium nanowires: Signatures of inelastic electron-boundary scattering in heat transfer, J. Low Temp. Phys. **189**, 204 (2017).